High Molecular Weight Protein-Like Semiflexible Chains via Bioorthogonal Polymerization of Coiled-Coil Peptides

Hanyuan Gao,[1] Tianren Zhang,[1,2] Matthew G. Langenstein,[1] Weiran Xie,[1] Samiksha Udan,[1] Zihan Zhang,[1] Jeffery G. Saven,[2] Shi Bai,[3] Darrin J. Pochan,[1] Joseph M. Fox,[1,3] Xinqiao Jia[1,4,5,6*]

[1]Department of Materials Science and Engineering, University of Delaware, Newark, DE, 19716, USA.

[2]Department of Chemistry, University of Pennsylvania, Philadelphia, PA, 19104, USA.

[3]Department of Chemistry and Biochemistry, University of Delaware, Newark, DE, 19716, USA.

[4]Department of Biomedical Engineering, University of Delaware, Newark, DE, 19716, USA.

[5]Department of Biological Sciences, University of Delaware, Newark, DE, 19716, USA.

[6]Delaware Biotechnology Institute, University of Delaware, Newark, DE, 19716, USA.

*Corresponding author, Email: xjia@udel.edu

Keywords: Coiled-coil peptides, tetrazine ligation, step growth polymerization, semiflexible, molecular weight, entanglement.

For Table of Contents Use Only

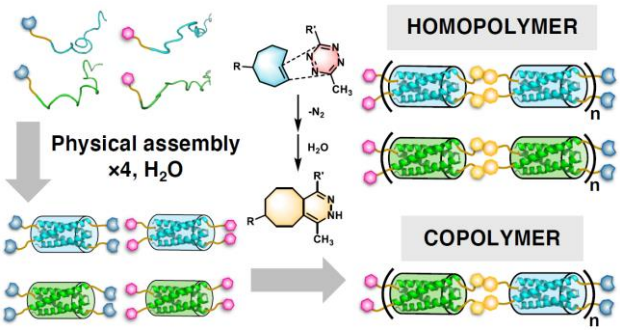

Tetrazine ligation-mediated step-growth polymerization of 4-helical coiled-coil bundles gives rise to exceptionally high molecular weight, protein-like polymers consisting of short oligoethylene glycol linkers interspersed between rigid coiled-coil domains.

ABSTRACT

Peptides capable of forming homotetrameric coiled-coil bundles are utilized as the monomeric building blocks (“bundlemers”) to synthesize protein-like hybrid polymers consisting of covalently linked coiled-coil microdomains with regularly spaced ethylene glycol repeats via step-growth polymerization employing the highly efficient, bioorthogonal tetrazine (Tz) ligation with *trans*-cyclooctene (TCO). Polymerization of Tz and TCO-functionalized peptides in aqueous media under strict stoichiometry at Tz or TCO concentrations of 0.1 to 4.5 mM leads to the establishment of exceptionally long, semiflexible polymer chains with a Kuhn length of 6-7 nm and an apparent molecular weight up to 3 MDa. Bioorthogonal polymerization at bundlemer concentrations above 5 mM gives rise to physical gels through interchain entanglements. Hydrogels prepared at 10 mM exhibit an average elastic modulus of 400 Pa and a strain to failure of 300%. Copolymerization of coiled-coil peptides with distinct composition and thermal stability results in hydrogels that are thermally tunable. Solid-to-fluid transition occurs when one of the coiled-coil repeats melts. Upon cooling, solid-like properties are partially recovered through intermolecular association of the helical peptides. Overall, tetrazine ligation has enabled the covalent polymerization of self-assembled coiled-coil motifs for the establishment of protein-like linear polymers with unprecedented molecular weight.

INTRODUCTION

The advances in organic chemistry, catalyst design, and polymerization methodologies have led to the development of a wide range of synthetic polymers with high molecular weight, variable composition and structure, and unique physical states and mechanical properties. Synthetic polymers, produced via step growth, chain growth or ring opening polymerization of small molecule compounds with chemically susceptible groups, consist of long chains of covalently linked monomeric repeat units.[1-4] With the exception of polypeptides and certain types of nonamide-based polymers, such as poly(isocyanide)s, poly(*p*-phenylenevinylene),[5] most synthetic polymers exist as random coils or extended chains; they normally do not fold into defined secondary structures seen in natural proteins. Although precise placement of reactive handles or hydrogen bonding units along the polymer backbone or at chain termini has enabled the creation of synthetic polymers with complex molecular architecture, shape, and morphology,[6-9] these nanoscale molecular structures lack the specificity, complexity, diversity, and flexibility seen in natural proteins.

Synthesized from natural amino acids through transcriptional and translational processes, proteins exhibit well-defined secondary, tertiary, and quaternary structures in aqueous media through concerted non-covalent interactions, including H-bonding, hydrophobic interactions, Van der Waals forces, and ionic interactions. The function of a particular protein is dependent on the peptide sequence as well as their unique higher-order structures.[10] To achieve diverse functions, many natural proteins contain multiple structurally and functionally distinct domains or motifs. For example, the giant muscle protein titin (~ 3 MDa) consists of multiple folded immunoglobulin domains arranged in series alternating with unstructured unique sequences.[11, 12] The consecutive and reversible unfolding and refolding of the domains are crucial for titin to serve as a modular spring.[13] On the other hand, structural proteins, such as keratins and vimentin, incorporate coiled-coil motifs, i.e. a superhelix of multiple α-helices twisted around each other, to provide mechanical strength to cells through the formation of rigid or semiflexible fibrous networks.[14]

The need for advanced materials with tunable properties and adaptive features has motivated researchers to exploit the utility of peptidic building blocks and motifs to create new materials with desired

functions.[15] Supramolecular polymerization of cyclic,[16] amphiphilic, and β sheet-forming peptides[17, 18] into ordered nanostructures has yielded materials with high molecular weight (~200 MDa[17]), long-range order, and enhanced tunability. Because the assembly is driven by non-covalent interactions, the structures and properties of this type of materials are dependent on pH, temperature and solvent conditions.[19, 20] To prevent the polymeric peptide assembly from dissociating, the constituent building blocks must exhibit high affinity for each other, thereby imparting mechanical properties similar to conventional polymers established entirely by covalent bonds.[21]

Peptide-based polymers can be synthesized through covalent coupling of pre-assembled peptidic motifs.[22, 23] The resultant hybrid materials retain the reversible and dynamic properties of supramolecular motifs, and at the same time are structurally sound and mechanically robust.[24] Side-chain-to-side-chain polymerization of vertically stacked cyclic β-peptide rings via the formation of amide linkages gives rise to nanofibers composed of a single polymer strand that is tougher than natural silk.[25] Alternatively, linker-free, end-to-end polymerization of antiparallel homotetrameric coiled-coil peptide bundles via thiol-Michael addition leads to the formation of hybrid polymers that are exceptionally rigid with persistence lengths up to 40 μm.[26] As one of the most abundant structural and functional motifs in nature, coiled-coils are essential for mediating strong and specific protein-protein interactions.[10] With a basic heptad repeat, the constituent peptides for coiled-coils can be computationally identified.[27]

To expand the range of material properties attainable by one-dimensional nanostructures, an alternative inter-bundle linking chemistry is explored for the preparation of polymeric coiled coils (PCCs). Herein, using customized, multistranded superhelices as unconventional monomers, we exploited the utility of tetrazine (Tz) ligation with *trans*-cyclooctene (TCO) for the preparation of semiflexible ultrahigh molecular weight PCCs. This reaction features fast kinetics, high selectivity at low concentrations, and compatibility with biological systems.[28, 29] We strategically introduced flexible oligoethylene glycol (OEG3-4) linkers between the peptide backbone and the bioorthogonal handles to afford semiflexible polymer chains. The PCCs were characterized experimentally and computationally to determine the secondary structure, diffusivity, molecular weight, and morphology. When polymerization was conducted at a

relatively high bundlemer concentration, interchain entanglement of ultrahigh molecular weight, semiflexible peptidic polymers gave rise to elastic hydrogels that are mechanically robust.

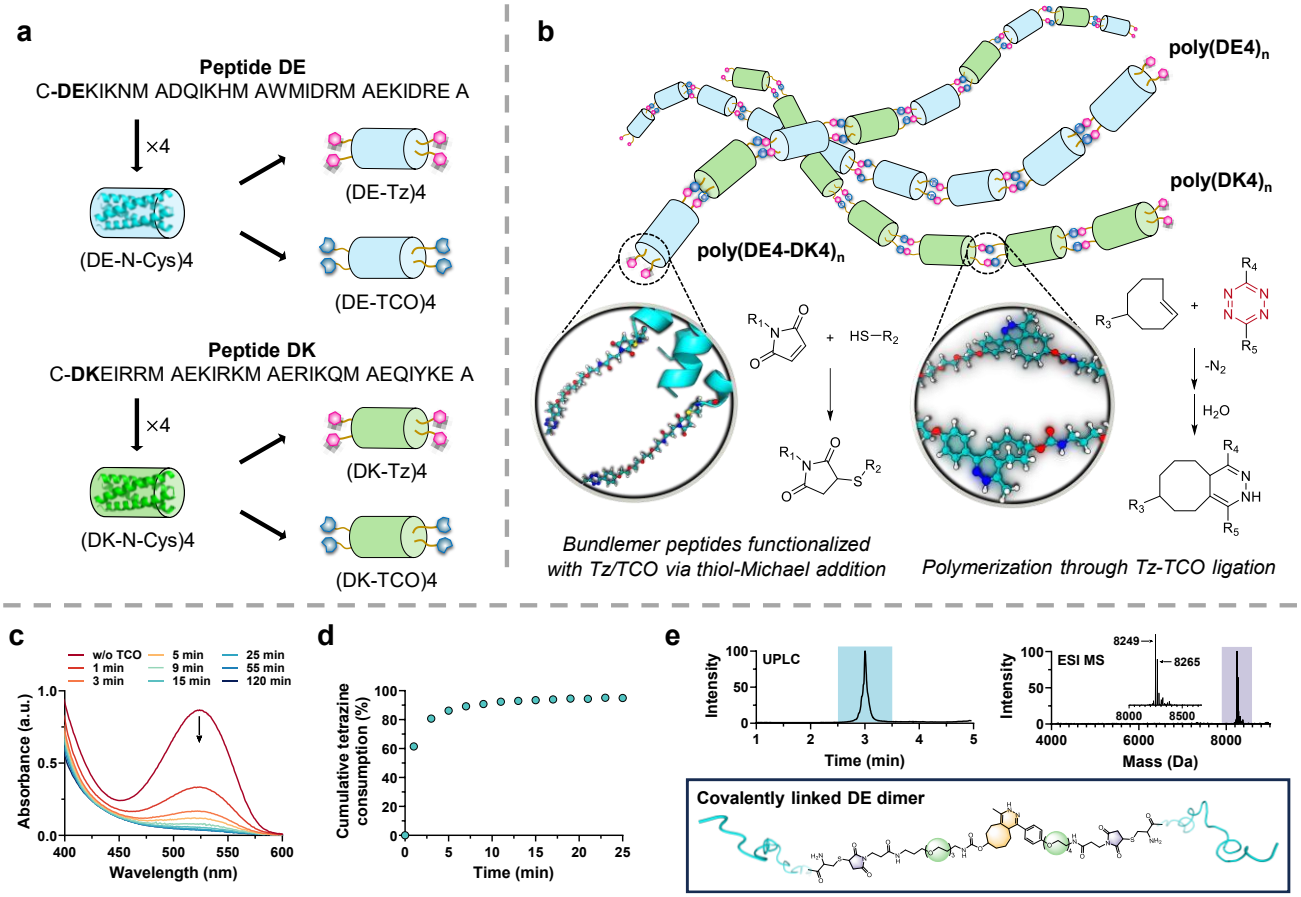

Figure 1. Bioorthogonal polymerization of coiled-coil peptides. a, Cysteine-tagged peptides, DE and DK, are used to prepare Tz and TCO-functionalized derivatives that assemble into four-helical coiled-coils under aqueous conditions. The bundlemer contains two bioorthogonal handles on each end. **b,** Tz and TCO groups are installed to the N-terminus of the peptide through thiol-Michael reaction and individual coiled-coils are linked together through the fast and highly efficient tetrazine-TCO ligation. **c,** Attenuation of the tetrazine chromophore at 524 nm during bioorthogonal polymerization as monitored by UV-vis spectroscopy. **d,** Cumulative tetrazine consumption during polymerization as a function of reaction time, showing 95% conversion of tetrazine to the cycloadduct 25 min after the supramolecular monomers were mixed at a Tz or TCO concentration of 2.5 mM. **e,** UPLC trace and deconvoluted ESI MS of poly(DE4)$_n$ showing the presence of peptide dimer after poly(DE4)$_n$ became denatured on the UPLC column. The second highest mass peak (M+16) is likely due to methionine oxidation. Figures were created using AlphaFold2,[30] Avogadro,[31] and BioRender.com.

RESULTS AND DISCUSSION

Formation of high molecular weight, semiflexible PCC rods.

We have successfully applied tetrazine/TCO ligation, an inverse electron demand Diels-Alder reaction with a second order rate constant $k_2 > 10^3$ $M^{-1}s^{-1}$,[28, 32] to synthesize mechanically robust hydrogel fibers via step-growth polymerization using traditional poly(ethylene glycol)-based monomers.[33-35] In this study, computationally designed peptides ("DE" and "DK", Figure 1a) that form stable antiparallel homotetrameric bundles [(DE)4 and (DK)4][26, 36, 37] were chosen as supramolecular monomers to produce PCCs via covalent step growth polymerization (Figure 1b). A cysteine residue was appended to the basic sequence at the N-terminus, through which Tz or TCO functionality was introduced using maleimide-OEG4-tetrazine and maleimide-OEG3-TCO, respectively (Figures S1-12). When assembled in H_2O, the bundlemers contain precisely four identical functional groups evenly distributed on each end. Homopolymers were prepared using the DE peptide at a Tz/TCO molar ratio of 1/1 and monomer concentrations of 1.0 - 4.5 mM. At 2.5 mM, ~60% of tetrazine was consumed one minute after mixing, as shown by the attenuation of the absorbance of the tetrazine chromophore (524 nm, Figure 1c). Tetrazine consumption gradually leveled off after 10 min, and by 25 min, over 95% of tetrazine was converted to cycloadduct (Figure 1d). A single peak at an elution time of 3 min with a molecular mass of 8,249 Da was detected from ultra-performance liquid chromatography (UPLC)–tandem electrospray ionization mass spectrometry (ESI-MS, Figure 1e, Figure S13). During the experiment, all constituent bundles were denatured by acetonitrile, causing the polymer to dissociate into covalently linked dimeric peptides that were readily detectable. Overall, our results confirmed the accessibility of the bioorthogonal reactive groups and the high efficiency of the cycloaddition reaction.

Dilute solution viscometry was employed to indirectly assess the size of poly$(DE4)_n$ under native conditions that preserve the secondary structure of the bundles. All measurements were performed in a good solvent (water) under a dilution solution regime with the polymer properly solvated, as evidenced by a logarithmic fit with a slope (concentration exponent) of ~ 1.3 [38-40] (Figure 2a), and negative Kraemer

constant K_K[41] (Table S1). Intrinsic viscosity ([η]) was determined by fitting inherent and reduced viscosity to Huggins[42] and Kreamer[43] Equations (Figure S14). As expected, the intrinsic viscosity of poly(DE4)$_n$ was significantly higher than that for the monomeric bundlemers (DE-Tz)4 and (DE-TCO)4 (Figure 2b). Moreover, the intrinsic viscosity increased with the bundlemer concentration used during polymerization.

Because the translational diffusion coefficient of a molecular species is directly related to its molecular weight, we next employed diffusion-ordered spectroscopy (DOSY) to assess poly(DE4)$_n$ molecular

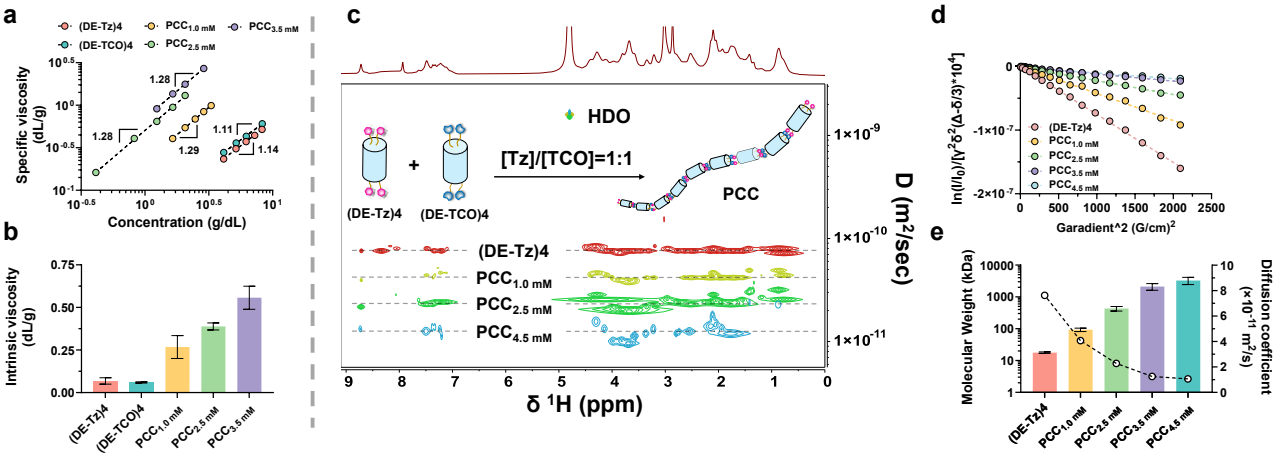

Figure 2. Evaluation of poly(DE4)$_n$ molecular weight by dilute solution viscometry and diffusion-ordered NMR spectroscopy. a, Specific viscosity as a function of solute concentration, confirming the maintenance of dilute solution regime. PCC was prepared at a Tz or TCO concentration of 1.0 ($PCC_{1.0\ mM}$), 2.5 ($PCC_{2.5\ mM}$) and 3.5 mM ($PCC_{3.5mM}$). **b,** Intrinsic viscosity for (DE-Tz)4, (DE-TCO)4, and poly(DE4)$_n$ prepared at various Tz/TCO concentrations (1.0, 2.5 and 3.5 mM). Error represents standard deviation. n = 3. **c,** Stacked 2D DOSY spectra for monomer (DE-Tz)4 and PCC synthesized at various Tz/TCO concentrations (1.0, 2.5 and 4.5 mM). The X-axis is the chemical shifts of ^{1}H (ppm) and the Y-axis is the diffusion coefficient (m^2/sec). D_2O is used as the internal reference for viscosity control during the measurement. **d,** Log plot of DOSY intensity attenuation at 3.97 - 3.99 ppm as a function of gradient squared for (DE-Tz)4 and PCC synthesized at various Tz/TCO concentrations. Data is fitted to the Stejskal-Tanner equation and the slope of the decay curve represents the diffusion coefficient. **e,** Apparent molecular weight (bars) and diffusion coefficient (circles) for (DE-Tz)4 and PCC. Error represents standard deviation. n = 15. The molecular weight was determined by fitting the DOSY diffusion coefficient to the standard curve reported by Bodor and co-workers.[45]

weight under native conditions. In this experiment, the NMR signal attenuates as the applied magnetic field gradient strength (g) increases, following the Stejskal–Tanner equation[44] with a linear correlation between the logarithm of signal intensity (I/I_0) and g^2, the slope of which indicates self-diffusion coefficient (D_{DOSY}) (Figure 2d). The Stejskal–Tanner plot for signals from the aliphatic, aromatic, and amide regions all decayed linearly (Figure S15) for both the monomeric and polymeric species. D_{DOSY} decreased progressively from the monomer to the polymer and PCCs prepared at a higher bundlemer concentration had a lower D_{DOSY} value (Table S2). In Figure 2c and Figure S16, 2D DOSY spectra for monomer (DE-Tz)4 and poly(ED4)$_n$ prepared at Tz (or TCO) concentrations of 1, 2.5 and 4.5 mM were overlaid for easy interpretation. In all experiments, the diffusion coefficient of the solvent (D_2O) was determined to be 1.62×10^{-9} m^2 s^{-1}, with a percent relative standard deviation of 4%, suggesting good viscosity control.[45] The DOSY cross-peaks of (DE-Tz)4 were well-defined in the diffusional dimension while those for poly(DE4)$_n$ prepared at higher Tz concentrations exhibited a relatively broader distribution, demonstrating a diversified range of polydispersity.[46]

The assembled tetrameric bundles and the OEG linkers mimic the rigid and flexible regions of folded proteins, respectively. Therefore, to estimate poly(DE4)$_n$ molecular weight, the average diffusion coefficient was fitted to a standard curve reported by Bodor[47] for folded proteins (Figure 2e, Table S2). This method is valid because fitting the standard curve with the diffusion coefficient of monomer (DE-Tz)4 yielded 17.7 kDa, very close to the actual molecular weight of the monomer (Table S2). Consistent with the viscometry results, poly(DE4)$_n$ prepared at a higher bundlemer concentration had a higher molecular weight. Importantly, polymerization at a Tz concentration of 4.5 mM led to the generation of poly(DE4)$_n$ with an apparent molecular weight of over 3 million Dalton, with close to 200 coiled-coil repeats, each over 16 kDa. As shown in Figure 1c-d, a significant amount of Tz was consumed immediately after (DE-Tz)4 and (DE-TCO)4 were mixed to produce PCC of low and intermediate molecular weight, forming two covalent linkages between neighboring bundles through end-to-end polymerization. The semiflexible nature of the PCC chains (see below) ensures an extended chain

structure with the reactive ends well exposed for continued monomer addition, producing PCCs with exceptionally high molecular weight.[33, 48-50]

The DE peptide is designed to exhibit an α-helical coiled-coil conformation with D_2 symmetry in water, detectable by circular dichroism (CD) as two minima at 208 and 222 nm.[51] Conjugation of Tz and TCO groups did not affect the ability of the peptide to self-assemble (Figure 3a, Figures S17-18). Both monomeric assemblies exhibited a melting temperature (T_m) of 50-60 °C, as determined by the

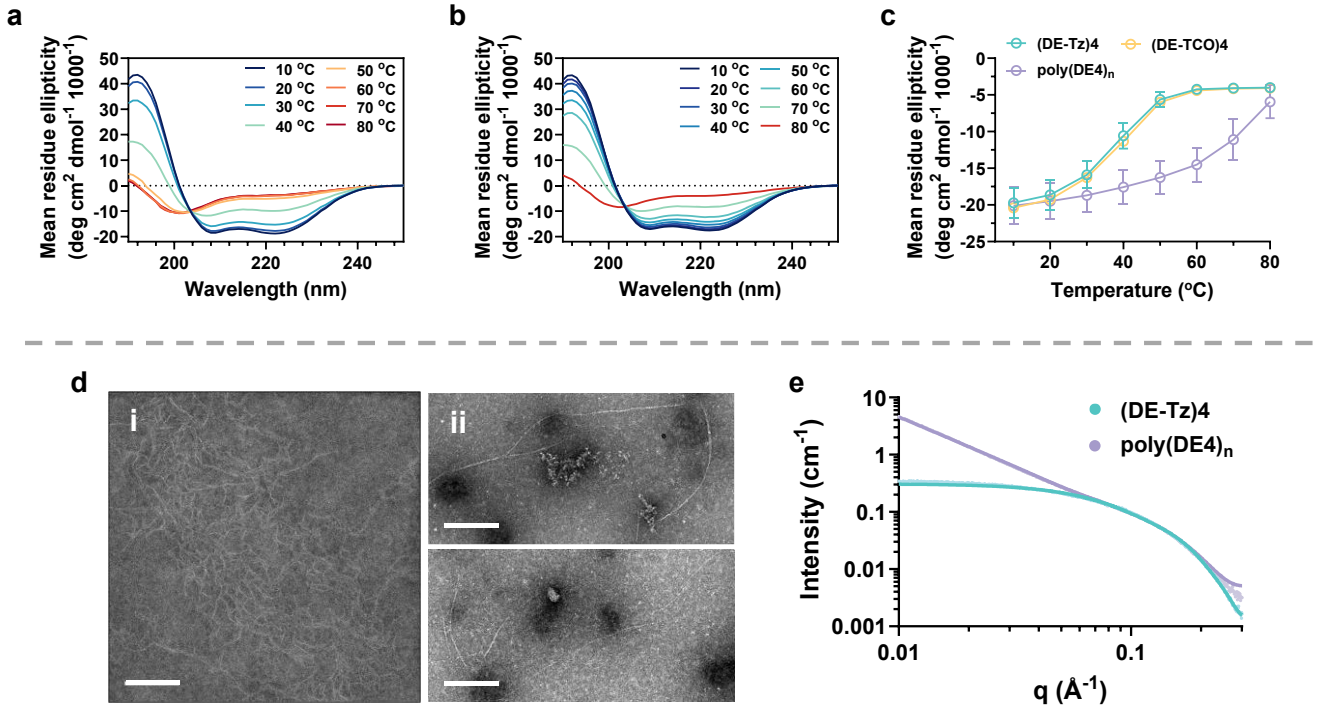

Figure 3. Characterization of the structure and morphology of poly(DE4)$_n$ by circular dichroism (CD, a-c), transmission electron microscopy (TEM, d) and small angle X-ray scattering (SAXS, e). **a,** Representative CD spectra of (DE-Tz)4 (a) and poly(DE4)$_n$ (b) showing mean residue ellipticity (MRE) as a function of wavelength and temperature. The presence of the two minima at 208 and 222 nm confirms the formation of the α-helical structure. **c,** Temperature-dependent MRE at 222 nm for (DE-Tz)4, (DE-TCO)4. The melting transition (T_m) for the coiled-coil building block is determined as 50-60 °C. **d,** Visualization of poly(DE4)$_n$ chains and aggregates by negative stain TEM. Poly(DE4)n in DI H_2O was either directly deposited on the TEM grid (i) or equilibrated in NaCl (1 M) prior to deposition (ii). Scale bar = 250 nm. **e,** SAXS data curved fitted to a rigid cylinder model for (DE-Tz)4 (cyan) and flexible cylinder model for poly(DE4)$_n$ (purple).

appearance of absorbance at 200 nm corresponding to a random coil, and the disappearance of the absorbance at 208 and 222 nm. Importantly, the secondary structure was preserved in the polymer product (Figure 3b). Comparison of the molar residue ellipticity (MRE) at 222 nm (Figure 3c) showed that poly(DE4)$_n$ denatures (i.e. denaturation of the helices) at a significantly higher temperature (70-80 °C) than the bundlemers (50-60 °C), suggesting stabilization of the helical conformation and strengthening of helix-to-helix association by covalent polymerization.[26, 52, 53]

Examination of the polymerization product, cast on the grid directly from H_2O, by transmission electron microscopy (TEM) with negative staining showed aggregates composed of semiflexible PCC chains (Figure 3d(i)). Examination under Cryo-TEM conditions also revealed substantional interchain association (Figure S21). Dilution and equilibration of poly(DE4)$_n$ in a NaCl solution prior to imaging signficantly reduced polymer aggregation by charge screening, revealing well-dispered single chains that appeared to be semiflexible (Figure 3d(ii)). This appearance is consistent with previously published semiflexible PCC chains prepared using maleimide functionalized bundlemer and tetrathiol pentaerythritol tetrakis(3-mercaptopropionate).[26] However, prior PCCs prepared using short length inter-bundle coupling chemistry resulted in the formation of stiff molecular fibers with rigid-rod behavior. Therefore, the physical characteristics of the hybrid polymer is dependent on inter-bundle linker chemistry.

Small angle X-ray scattering (SAXS) was used to determine Kuhn lengths and cross-section radii of poly(DE4)$_n$ (Figure 3e and Table S3). The (DE-Tz)4 building block fits reasonably well (reduced chi-squared, χ^2 = 1.43) to a cylinder model with a length of 6.7 nm and a radius of 1.2 nm. This radius is consistent with the values for previously published bundlemers, while the length is consistant with a typical bundlemer (l = 3.6 - 4.5 nm) [26, 36, 37, 54-56] plus extended OEG linkers at each N-termini. Treating poly(DE4)$_n$ as a series of rigid bundlemer segments connected by flexible OEG linkers, we fitted it to a flexible cylinder model in SASview as has been previously done for semiflexible bundlemer rods.[26, 56] Additionally, given the relatively long and flexible nature of the OEG linker, with a total of 7 ethylene oxide repeats between adjacent bundlers, it is unlikely for the polymer to have a singular fixed Kuhn length, but

instead a range of Kuhn lengths dependent on whether OEG is extended or collapsed. By fitting the Kuhn length with a Gaussian distribution (Figure S22), our analyses revealed that poly(DE4)$_n$ (reduced χ^2 = 1.12) had a radius of 1.3 nm and an average Kuhn length of 6.3 nm with a standard deviation of 1.3 nm. This Kuhn length is slightly smaller than the previously reported 7.1 ± 1 nm for semiflexible bundlemer chains[56] linked with a 4-arm PEG linker but is still indicative of a single bundlemer persistence length.

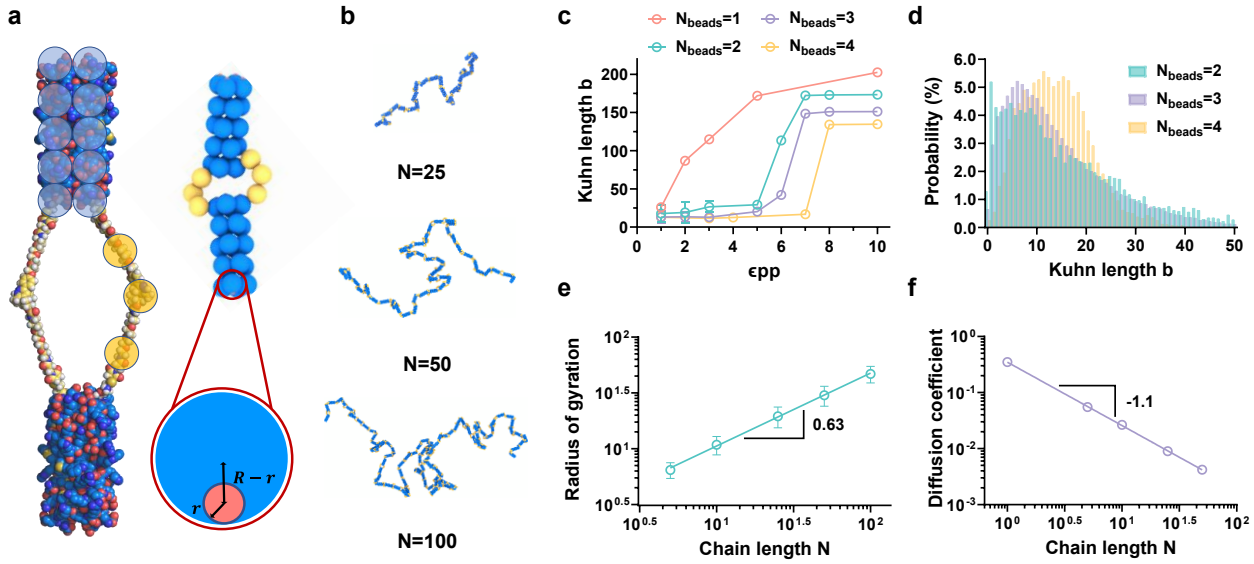

Figure 4. Coarse-grain (CG) modeling of polymeric coiled-coil peptides. a, All-atom and coarse-grained representations of a linked dimer system wherein $r = 0.1\sigma$, $R - r = 0.4\sigma$. **b,** CG chains with various number of bundlemer repeating units N and the length of linker is $N_{beads} = 3$. **c,** Average Kuhn length b for the CG systems with different N_{beads} values at various attractive terminus interactions ϵ_{pp}, and the chain length is fixed at N = 50. **d,** Kuhn length b distributions for the chains with different N_{beads} values at N = 50. **e,** Chain conformations, radius of gyration R_g, as a function of the chain length N, and $N_{beads} = 3$. **f,** Diffusion coefficient D as a function of chain length N at $N_{beads} = 3$. Error represents standard deviation. n = 3.

Separately, a coarse-grain (CG) model was employed to microscopically investigate the conformation of doubly linked bundlemer chains (Figure 4a-b). Based on the rigid rod chain extrapolated from our previous study,[26] attractive interactions among the terminal residues of bundlemers and the intervening chemical linkers are critical in determining the stiffness of the chain. Therefore, both terminus interaction energy, ϵ_{pp}, and the length of the linkers, N_{beads}, were varied to identify the most suitable parameters

that can capture chain properties observed in the experiments. Herein, the Kuhn length, b, related to the flexibility of the chains, served as a metric for comparison between simulations and experimental results. As shown in Figure 4c, a competing effect between N_{beads} and ϵ_{pp} was observed. For chains with $N_{beads} = 1$, the Kuhn length, b, continuously increased as the attractive interactions among the adjacent bundlemer termini became larger, ultimately reaching a plateau with increasing ϵ_{pp}, indicating rigid rod formation. In contrast, a sharp transition regime was observed for the chains with a longer linker. As we explored the low ϵ_{pp} range, the Kuhn length for both $N_{beads} = 3$ and $N_{beads} = 4$ with $\epsilon_{pp} = 1.0$ were similarly close to the experimentally measured results. Moreover, for $N_{beads} = 3$, the Kuhn length distribution plot (Figure 4d) shows the highest probability around 6.0 nm, in good agreement with SAXS analysis of experimentally produced chains in terms of local chain conformation.

We further interrogated the chain conformation of PCCs computationally by varying the number of bundlemer repeat unit N while keeping $N_{beads} = 3$ and $\epsilon_{pp} = 1.0$. From the scaling of the radius of gyration ($\mathrm{R_g}$) with N as $\mathrm{R_g}{\sim}\mathrm{N}^{\nu}$, the Flory exponent was determined as $\nu = 0.63$, suggesting that the modeled polymer chain was in good solvent with relatively extended conformations (Figure 4e). The calculated ratio $\frac{R_e^2}{R_g^2} \approx 6.7$, where end-to-end distance $R_e \approx 91$ for the chain with N = 100 was above the theoretical value 6.3 for flexible chain in a good solvent.[57] Furthermore, the diffusion coefficient D, calculated from the mean square displacement (MSD) (Figure S23) of PCC chains decreased as N increased (Figure 4f), which is consistent with experimental observations (Figure 2e). The scaling of D with N followed $D{\sim}N^{-1.1}$, which indicated a diffusive behavior within the Rouse regimes.[39] Overall, the simulations provide a molecular picture that PCCs consisting of covalently linked coiled-coil bundles behave like semiflexible polymers, even though the constituent bundlemer building blocks are inherently rigid, due to the presence of flexible OEG linkers between neighboring bundles.

PCC hydrogels via interchain entanglements

When polymerization was conducted at a Tz concentration of 5 mM, a transparent hydrogel with a yellow tint was obtained (Figure 5a-b, Video S1). The distinct pink-red color associated with the tetrazine chromophore disappeared rather rapidly (within minutes) after (DE-TCO)4 and (DE-Tz)4 were mixed. Characterization by oscillatory rheometry indicated a liquid-to-solid transition at 5 min (Figure S24a), with

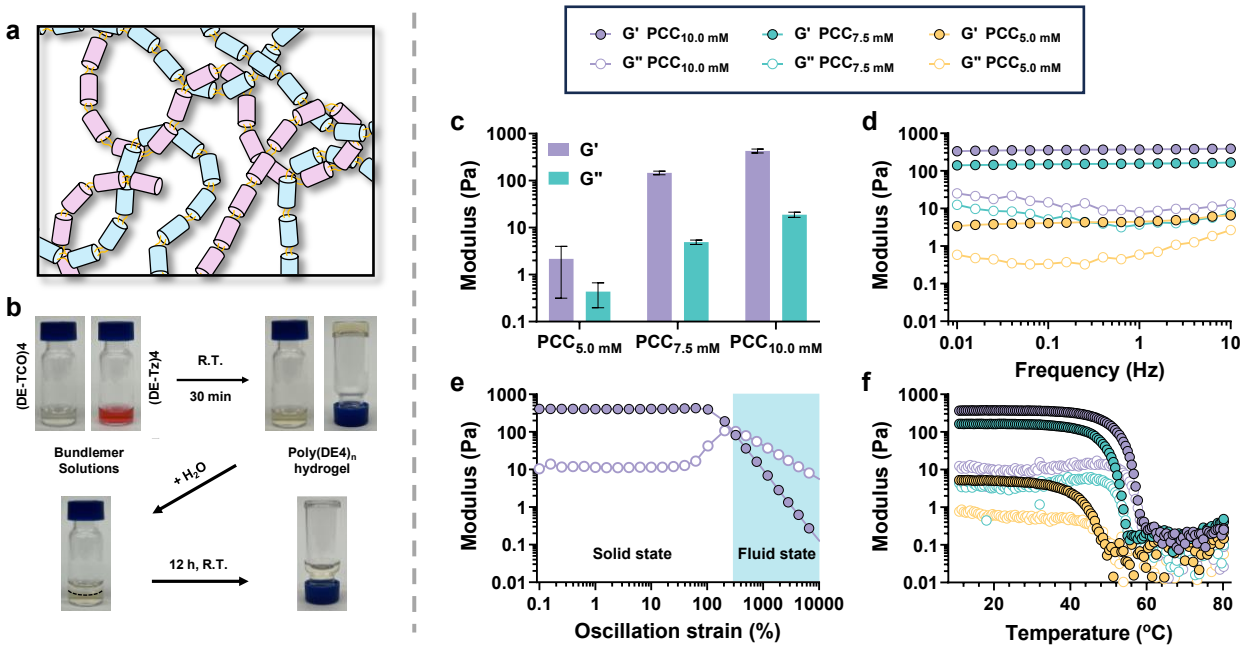

Figure 5. PCC hydrogels via intermolecular entanglement. a, Schematic illustration of polymeric coiled-coil hydrogels via the entanglement of semiflexible polymer chains. Neighboring chains are contrasted in pink and cyan for easy interpretation. **b,** Vial inversion experiment showing hydrogel formation after mixing of bioorthogonally functionalized coiled-coil peptides at a Tz/TCO ratio of 1:1 and hydrogel dissolution after the addition of water and overnight equilibration. **c,** Bioorthogonal polymerization at a higher bundlemer concentration leads to the establishment of stiffer hydrogel. The elastic (G') and loss (G") moduli are determined from the time sweep experiment at 1 Hz and 1% strain. Error represents standard deviation. n = 3. **d,** Hydrogel stiffness is independent of oscillatory frequency. Frequency sweep experiments are conducted from 0.01 to 10 Hz with a fixed strain of 1%. **e,** High oscillatory strain (~300%) is required to convert the elastic solid to a liquid. The crossover point of G' and G" indicates the transition from solid to fluid states. The amplitude sweep experiments were performed at a fixed frequency at 1 Hz on hydrogels prepared at a Tz/TCO concentration of 10 mM. **f,** Storage and loss moduli of peptidic hydrogels as a function of temperature. The crossover points of G' and G" represent the melting temperature of hydrogels.

the storage modulus (G') significantly higher than the loss modulus (G"). After 20 min of polymerization, both G' and G" values reached a plateau. The gelation kinetics and hydrogel stiffness are strongly dependent on the Tz concentration in feed (Figure 5c, Figure S24). When polymerization was conducted at a Tz concentration of 10 mM, hydrogels reached a G' of ~400 Pa. Although the supramolecular bundlemer building blocks are tetrafunctional, branching and crosslinking via the formation of a stable cycloaddition adduct is not possible owing to the high rigidity of the antiparallel homotetrameric coiled-coils.[26] Once one covalent bond between the bundlemers has formed, a second reaction between the same pair is highly likely due to the proximity of the functional groups. Although the Tz/TCO reaction sites are separated from the ends of the rigid bundlemers by OEG7, these linkages are not sufficiently long to enable branching. As discussed above, owing to the presence of flexible OEG linkers between each bundle, these hybrid polymers exhibited high chain flexibility. Thus, we reason that hydrogel formation is a direct result of physical entanglement of ultrahigh molecular weight PCCs. This hypothesis is supported by our experimental observations; addition of copious amount of water to the as-synthesized hydrogel led to complete dissolution overnight (Figure 5b).

We further analyzed the viscoelastic properties of these hydrogels over a wide range of frequencies (Figure 5d) and strains (Figure S25). The storage modulus remained constant at frequencies of 0.01-10 Hz and oscillation strain of 1%, indicating that the physical entanglement is long-lived. Unlike other entangled hydrogels that fail at very low strains,[23] this type of non-covalent hydrogel exhibits a solid-to-fluid transition at 300% strain (Figure 5e) that is attributable to the disentanglement of polymer chains. Solid-to-fluid transition was also observed with increasing temperature, and the transition occurred at a higher temperature for gels prepared at a higher Tz concentration in feed (Figure 5f). We hypothesized that as the temperature increased, poly(DE4)$_n$ became partially denatured via the disassembly of individual bundles, yielding low molecular weight, covalently coupled peptide homodimers (Figure 6a) that are unable to entangle.[58, 59] When the peptide solution was subsequently cooled down to 10 °C, we did not observe any gel formation (Figure 6b-d).

To further demonstrate the versatility of the bioorthogonal strategy, (DE-Tz)4 was copolymerized with (DK-TCO)4 (Figure 1a, Figures S7-12) that is compositionally distinct and thermally more stable (T_m = 70-80 °C, Figures S19-20). Polymerization at 10 mM led to the rapid formation of a physical gel with G' ~1,000 Pa (Figure 6e-h), presumably through the entanglement of high molecular weight poly(DE4-DK4)$_n$. When heated to 60 °C, G' gradually dropped below 100 Pa while G" increased to just over 100 Pa, indicating transformation to a fluid (Figure 6f). Upon cooling to 10 °C, a sol-gel transition was observed, giving rise to a softer gel (G' = 200 Pa). The copolymer system can withstand multiple heating and cooling cycles with partial recovery of the initial gel stiffness. By the end of the 10th cycle, the recovered gel had a G' and G" of 20 and 2 Pa, respectively (Figure 6f-h). Exposure of poly(DK4)$_n$ to the same heating/cooling regimen (60-10 °C) did not significantly alter the mechanical integrity of the hydrogel (Figure S26). However, cycling between 80 and 10 °C led to permanent disintegration of the network structure (Figure S27).

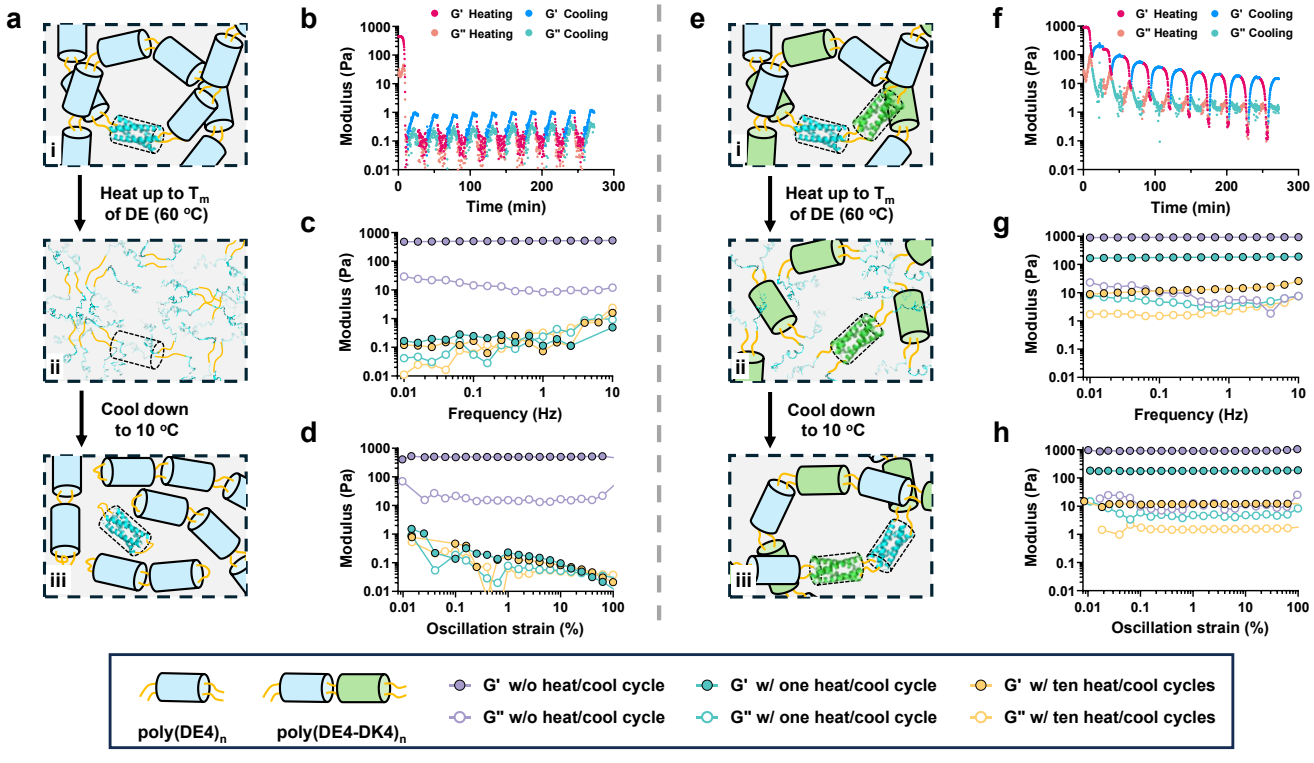

Figure 6. Effects of cyclic heating/cooling between 60 °C (T_m of DE4) and 10 °C on the mechanical properties of poly(DE4)$_n$ and poly(ED4-DK4)$_n$ hydrogels. **a,** Proposed molecular structure of poly(DE4)$_n$

hydrogels at ambient temperature (i), after heating to 60 °C (ii) and then cooling down to 10 °C (iii). **b,** Storage (G') and loss moduli (G") were plotted as a function of time under temperature cycling. Time sweep experiments were conducted at a frequency of 0.1 Hz and a strain of 0.5%. The temperature was ramped up to 60 °C at 5 °C/min, held constant for 2 min, then ramped down at the same speed and held constant for 5 min. **c,** Storage (G') and loss moduli (G") were plotted as a function of frequency at a constant strain of 0.5% for hydrogels initially formed (purple), after the 1st (cyan) and the 10th (orange) heating/cooling cycle. **d,** Storage (G') and loss moduli (G") were plotted as a function of strain at a constant frequency of 0.1 Hz for hydrogels initially formed (purple), after the 1st (cyan) and the 10th (orange) heating/cooling cycles. **e,** Proposed molecular structure of poly(DE4)$_n$ hydrogels at ambient temperature (i), after heating to 60 °C (ii) and then cooling down to 10 °C (iii). **f,** Storage (G') and loss moduli (G") were plotted as a function of time under temperature cycling. Time sweep experiments were conducted at a frequency of 0.1 Hz and a strain of 0.5%. The temperature was ramped up to 60 °C at 5 °C/min, held constant for 2 min, then ramped down at the same speed and held constant for 5 min. **g,** Storage (G') and loss moduli (G") were plotted as a function of frequency at a constant strain of 0.5% for hydrogels initially formed (purple), after the 1st (cyan) and the 10th (orange) heating/cooling cycle. **h,** Storage (G') and loss moduli (G") were plotted as a function of strain at a constant frequency of 0.1 Hz for hydrogels initially formed (purple), after the 1st (cyan) and the 10th (orange) heating/cooling cycles. Figures were created using AlphaFold2[30] and BioRender.com.

We speculate that at 60 °C, only the DE4 units were denatured; during the cooling cycle, the intact DK4 bundles serve as templates for the association of neighboring DE peptides, leading to the growth of high molecular weight products. However, when the neighboring units are not perfectly aligned, network defects are generated due to the inability of the DE peptides to re-assemble. Repeated heating and cooling results in the accumulation of network defects, compromising the overall hydrogel mechanical properties. This is not the case for the homodimeric hydrogel system. At 60 °C, poly(DE4)$_n$ dissociates to peptide dimers covalently coupled through a flexible OEG7 linker (Figure 1e, Figure S26). To re-establish the molecular structure of the "homopolymer" at 10 °C, four dimeric units must re-assemble in an antiparallel fashion to allow supramolecular polymerization. The flexible OEG7 linker between the two identical peptides permits intramolecular association through back folding, resulting in the formation of a

“molecular capper” that distorts the overall reaction stoichiometry and prevents the restoration of the entangled network structure.

CONCLUSION

In summary, the rapid and highly efficient tetrazine-TCO ligation enabled the synthesis of polymeric coiled-coils with exceptional molecular weight. The long chain hybrid polymer produced at a bundlemer concentration of 4.5 mM consists of up to 200 covalently linked rigid 4-helical peptide bundles. Unlike the stiff, rod-like polymeric coiled-coils reported previously, the hybrid polymers developed here are semiflexible owing to the presence of defined PEG linkers between adjacent bundles. Polymerization at a monomer concentration greater than 4.5 mM resulted in hydrogel formation through the entanglement of the semiflexible polymer chains. The hybrid polymer recapitulated key features of supramolecular polymers, including dynamic and reversible properties, and at the same time, exhibited the robustness and stability of conventional covalently linked polymers. Physical gels established through intermolecular entanglements of the semiflexible polymeric chains behave like covalent networks. While conventional flexible polymers unentangle readily through reptation, semiflexible chains disentangle due to correlated constraint release, which leads to equilibration of internal bending modes before polymers diffuse the full tube length.[60] The bioorthogonality of tetrazine ligation allows the synthesis of new nanometer-scale structures by combining bundlemer building blocks with diverse functionalities and structures. Given the tunability of stiffness and thermodynamic reversibility, the hybrid hydrogel system investigated here may find applications in 3D printing, cell culture, and drug release.

Supporting information.

Synthetic procedures, characterization methods, coarse grain simulation, supplemental figures.

Acknowledgements.

This research was primarily/partially supported by the National Science Foundation (NSF) through the University of Delaware Materials Research Science and Engineering Center DMR-2011824. Additional support was received from the National Institutes of Health (NIDCD, R01DC014461; NIDCR R01DE029655), NSF (DMR 1809612), and Delaware Bioscience Center for Advanced Technology (DE-CAT 12A00448). Support was also provided by the Department of Energy (DOE) Office of Basic Energy Sciences, Biomolecular Materials Program under grant No. DE-SC0019355. Additional support for the simulation of solution behavior was provided under award DE-SC0019282. Computational studies were performed using allocation TG-CHE110041 from the Advanced Cyberinfrastructure Coordination Ecosystem: Services & Support (ACCESS) program, which is supported by National Science Foundation grants #1548562, #2138259, #2138286, #2138307, #2137603, and #2138296.

References

(1) Odian, G. *Principles of Polymerizaation*; John Wiley & Sons, 2004.

(2) Ouchi, M.; Terashima, T.; Sawamoto, M. Precision control of radical polymerization via transition metal catalysis: from dormant species to designed catalysts for precision functional polymers. *Acc Chem Res* **2008**, *41* (9), 1120-1132. DOI: 10.1021/ar800063t From NLM.

(3) Worch, J. C.; Dove, A. P. Click Step-Growth Polymerization and E/Z Stereochemistry Using Nucleophilic Thiol-yne/-ene Reactions: Applying Old Concepts for Practical Sustainable (Bio)Materials. *Acc Chem Res* **2022**, *55* (17), 2355-2369. DOI: 10.1021/acs.accounts.2c00293 From NLM.

(4) Honda, S.; Odelius, K.; Sardon, H. Organomediated polymerization. *Communications Chemistry* **2024**, *7* (1), 62. DOI: 10.1038/s42004-024-01134-1.

(5) Milton, M.; Deng, R.; Mann, A.; Wang, C.; Tang, D.; Weck, M. Secondary Structure in Nonpeptidic Supramolecular Block Copolymers. *Acc Chem Res* **2021**, *54* (10), 2397-2408. DOI: 10.1021/acs.accounts.1c00028 From NLM.

(6) Harth, E.; Van Horn, B.; Lee, V. Y.; Germack, D. S.; Gonzales, C. P.; Miller, R. D.; Hawker, C. J. A facile approach to architecturally defined nanoparticles via intramolecular chain collapse. *J Am Chem Soc* **2002**, *124* (29), 8653-8660. DOI: 10.1021/ja026208x From NLM.

(7) Foster, E. J.; Berda, E. B.; Meijer, E. W. Metastable supramolecular polymer nanoparticles via intramolecular collapse of single polymer chains. *J Am Chem Soc* **2009**, *131* (20), 6964-6966. DOI: 10.1021/ja901687d From NLM.

(8) Schmidt, B. V.; Fechler, N.; Falkenhagen, J.; Lutz, J. F. Controlled folding of synthetic polymer chains through the formation of positionable covalent bridges. *Nat Chem* **2011**, *3* (3), 234-238. DOI: 10.1038/nchem.964 From NLM.

(9) Mato, Y.; Honda, K.; Ree, B. J.; Tajima, K.; Yamamoto, T.; Deguchi, T.; Isono, T.; Satoh, T. Programmed folding into spiro-multicyclic polymer topologies from linear and star-shaped chains. *Communications Chemistry* **2020**, *3* (1), 97. DOI: 10.1038/s42004-020-00355-4.

(10) Alberts, B.; Johnson, A.; Lewis, J.; Raff, M.; Roberts, K.; Walter, P. *Molecular Biology of the Cell*; Garland Science, 2002.

(11) Trinick, J. Cytoskeleton: Titin as a scaffold and spring. *Current Biology* **1996**, *6* (3), 258-260. DOI: https://doi.org/10.1016/S0960-9822(02)00472-4.

(12) Tskhovrebova, L.; Trinick, J. Titin: properties and family relationships. *Nature Reviews Molecular Cell Biology* **2003**, *4* (9), 679-689. DOI: 10.1038/nrm1198.

(13) Wang, K.; Forbes, J. G.; Jin, A. J. Single molecule measurements of titin elasticity. *Prog Biophys Mol Biol* **2001**, *77* (1), 1-44. DOI: 10.1016/s0079-6107(01)00009-8 From NLM.

(14) Eldirany, S. A.; Lomakin, I. B.; Ho, M.; Bunick, C. G. Recent insight into intermediate filament structure. *Curr Opin Cell Biol* **2021**, *68*, 132-143. DOI: 10.1016/j.ceb.2020.10.001 From NLM.

(15) Webber, M. J.; Appel, E. A.; Meijer, E. W.; Langer, R. Supramolecular biomaterials. *Nature Materials* **2016**, *15* (1), 13-26. DOI: 10.1038/nmat4474.

(16) Hu, K.; Jiang, Y.; Xiong, W.; Li, H.; Zhang, P.-Y.; Yin, F.; Zhang, Q.; Geng, H.; Jiang, F.; Li, Z.; et al. Tuning peptide self-assembly by an in-tether chiral center. *Science Advances* **2018**, *4* (5), eaar5907. DOI: 10.1126/sciadv.aar5907 (acccessed 2023/11/26).

(17) Hartgerink, J. D.; Beniash, E.; Stupp, S. I. Self-Assembly and Mineralization of Peptide-Amphiphile Nanofibers. *Science* **2001**, *294* (5547), 1684-1688. DOI: 10.1126/science.1063187 (acccessed 2023/11/26).

(18) Cui, H.; Cheetham, A. G.; Pashuck, E. T.; Stupp, S. I. Amino Acid Sequence in Constitutionally Isomeric Tetrapeptide Amphiphiles Dictates Architecture of One-Dimensional Nanostructures. *Journal of the American Chemical Society* **2014**, *136* (35), 12461-12468. DOI: 10.1021/ja507051w.

(19) Yuan, C.; Ji, W.; Xing, R.; Li, J.; Gazit, E.; Yan, X. Hierarchically oriented organization in supramolecular peptide crystals. *Nature Reviews Chemistry* **2019**, *3* (10), 567-588. DOI: 10.1038/s41570-019-0129-8.

(20) Sinha, N. J.; Langenstein, M. G.; Pochan, D. J.; Kloxin, C. J.; Saven, J. G. Peptide Design and Self-assembly into Targeted Nanostructure and Functional Materials. *Chemical Reviews* **2021**, *121* (22), 13915-13935. DOI: 10.1021/acs.chemrev.1c00712.
(21) de Greef, T. F. A.; Meijer, E. W. Supramolecular polymers. *Nature* **2008**, *453* (7192), 171-173. DOI: 10.1038/453171a.
(22) Tang, W.; Becker, M. L. "Click" reactions: a versatile toolbox for the synthesis of peptide-conjugates. *Chemical Society Reviews* **2014**, *43* (20), 7013-7039, 10.1039/C4CS00139G. DOI: 10.1039/C4CS00139G.
(23) Li, C.; Iscen, A.; Sai, H.; Sato, K.; Sather, N. A.; Chin, S. M.; Álvarez, Z.; Palmer, L. C.; Schatz, G. C.; Stupp, S. I. Supramolecular–covalent hybrid polymers for light-activated mechanical actuation. *Nature Materials* **2020**, *19* (8), 900-909. DOI: 10.1038/s41563-020-0707-7.
(24) Zhang, X. Supramolecular Polymer Chemistry: Past, Present, and Future. *Chinese Journal of Polymer Science* **2022**, *40* (6), 541-542. DOI: 10.1007/s10118-022-2748-7.
(25) Fears, K. P.; Kolel-Veetil, M. K.; Barlow, D. E.; Bernstein, N.; So, C. R.; Wahl, K. J.; Li, X.; Kulp, J. L.; Latour, R. A.; Clark, T. D. High-performance nanomaterials formed by rigid yet extensible cyclic β-peptide polymers. *Nature Communications* **2018**, *9* (1), 4090. DOI: 10.1038/s41467-018-06576-5.
(26) Wu, D.; Sinha, N.; Lee, J.; Sutherland, B. P.; Halaszynski, N. I.; Tian, Y.; Caplan, J.; Zhang, H. V.; Saven, J. G.; Kloxin, C. J.; et al. Polymers with controlled assembly and rigidity made with click-functional peptide bundles. *Nature* **2019**, *574* (7780), 658-662. DOI: 10.1038/s41586-019-1683-4.
(27) Woolfson, D. N. Coiled-Coil Design: Updated and Upgraded. *Subcell Biochem* **2017**, *82*, 35-61. DOI: 10.1007/978-3-319-49674-0_2 From NLM.
(28) Blackman, M. L.; Royzen, M.; Fox, J. M. Tetrazine ligation: fast bioconjugation based on inverse-electron-demand Diels-Alder reactivity. *J Am Chem Soc* **2008**, *130* (41), 13518-13519. DOI: 10.1021/ja8053805 From NLM.
(29) Scinto, S. L.; Bilodeau, D. A.; Hincapie, R.; Lee, W.; Nguyen, S. S.; Xu, M.; am Ende, C. W.; Finn, M. G.; Lang, K.; Lin, Q.; et al. Bioorthogonal chemistry. *Nature Reviews Methods Primers* **2021**, *1* (1), 30. DOI: 10.1038/s43586-021-00028-z.
(30) Jumper, J.; Evans, R.; Pritzel, A.; Green, T.; Figurnov, M.; Ronneberger, O.; Tunyasuvunakool, K.; Bates, R.; Žídek, A.; Potapenko, A.; et al. Highly accurate protein structure prediction with AlphaFold. *Nature* **2021**, *596* (7873), 583-589. DOI: 10.1038/s41586-021-03819-2.
(31) Hanwell, M. D.; Curtis, D. E.; Lonie, D. C.; Vandermeersch, T.; Zurek, E.; Hutchison, G. R. Avogadro: an advanced semantic chemical editor, visualization, and analysis platform. *Journal of Cheminformatics* **2012**, *4* (1), 17. DOI: 10.1186/1758-2946-4-17.
(32) Dicker, K. T.; Song, J.; Moore, A. C.; Zhang, H.; Li, Y.; Burris, D. L.; Jia, X.; Fox, J. M. Core-shell patterning of synthetic hydrogels via interfacial bioorthogonal chemistry for spatial control of stem cell behavior. *Chem Sci* **2018**, *9* (24), 5394-5404. DOI: 10.1039/c8sc00495a From NLM.
(33) Liu, S.; Zhang, H.; Remy, R. A.; Deng, F.; Mackay, M. E.; Fox, J. M.; Jia, X. Meter-long multiblock copolymer microfibers via interfacial bioorthogonal polymerization. *Adv Mater* **2015**, *27* (17), 2783-2790. DOI: 10.1002/adma.201500360 From NLM.
(34) Liu, S.; Moore, A. C.; Zerdoum, A. B.; Zhang, H.; Scinto, S. L.; Zhang, H.; Gong, L.; Burris, D. L.; Rajasekaran, A. K.; Fox, J. M.; et al. Cellular interactions with hydrogel microfibers synthesized via interfacial tetrazine ligation. *Biomaterials* **2018**, *180*, 24-35. DOI: 10.1016/j.biomaterials.2018.06.042 From NLM.
(35) George, O. J.; Song, J.; Benson, J. M.; Fang, Y.; Zhang, H.; Burris, D. L.; Fox, J. M.; Jia, X. Tunable Synthesis of Hydrogel Microfibers via Interfacial Tetrazine Ligation. *Biomacromolecules* **2022**, *23* (7), 3017-3030. DOI: 10.1021/acs.biomac.2c00504.
(36) Zhang, H. V.; Polzer, F.; Haider, M. J.; Tian, Y.; Villegas, J. A.; Kiick, K. L.; Pochan, D. J.; Saven, J. G. Computationally designed peptides for self-assembly of nanostructured lattices. *Sci Adv* **2016**, *2* (9), e1600307. DOI: 10.1126/sciadv.1600307 From NLM.

(37) Guo, R.; Sinha, N. J.; Misra, R.; Tang, Y.; Langenstein, M.; Kim, K.; Fagan, J. A.; Kloxin, C. J.; Jensen, G.; Pochan, D. J.; et al. Computational Design of Homotetrameric Peptide Bundle Variants Spanning a Wide Range of Charge States. *Biomacromolecules* **2022**, *23* (4), 1652-1661. DOI: 10.1021/acs.biomac.1c01539.
(38) Morris, E. R.; Cutler, A. N.; Ross-Murphy, S. B.; Rees, D. A.; Price, J. Concentration and shear rate dependence of viscosity in random coil polysaccharide solutions. *Carbohydrate Polymers* **1981**, *1* (1), 5-21. DOI: https://doi.org/10.1016/0144-8617(81)90011-4.
(39) Rubinstein, M.; Colby, R. H. *Polymer physics*; Oxford university press,, 2003.
(40) Shahbazi, M.; Jäger, H.; Ettelaie, R.; Chen, J. Construction of 3D printed reduced-fat meat analogue by emulsion gels. Part I: Flow behavior, thixotropic feature, and network structure of soy protein-based inks. *Food Hydrocolloids* **2021**, *120*, 106967. DOI: https://doi.org/10.1016/j.foodhyd.2021.106967.
(41) O'Sullivan, J.; Murray, B.; Flynn, C.; Norton, I. The effect of ultrasound treatment on the structural, physical and emulsifying properties of animal and vegetable proteins. *Food Hydrocolloids* **2016**, *53*, 141-154. DOI: https://doi.org/10.1016/j.foodhyd.2015.02.009.
(42) Huggins, M. L. The Viscosity of Dilute Solutions of Long-Chain Molecules. IV. Dependence on Concentration. *Journal of the American Chemical Society* **1942**, *64* (11), 2716-2718. DOI: 10.1021/ja01263a056.
(43) Kraemer, E. O. Molecular Weights of Celluloses and Cellulose Derivates. *Industrial & Engineering Chemistry* **1938**, *30* (10), 1200-1203. DOI: 10.1021/ie50346a023.
(44) Stejskal, E. O.; Tanner, J. E. Spin Diffusion Measurements: Spin Echoes in the Presence of a Time-Dependent Field Gradient. *The Journal of Chemical Physics* **1965**, *42* (1), 288-292. DOI: 10.1063/1.1695690 (acccessed 5/1/2024).
(45) Li, W.; Chung, H.; Daeffler, C.; Johnson, J. A.; Grubbs, R. H. Application of 1H DOSY for Facile Measurement of Polymer Molecular Weights. *Macromolecules* **2012**, *45* (24), 9595-9603. DOI: 10.1021/ma301666x.
(46) Viéville, J.; Tanty, M.; Delsuc, M.-A. Polydispersity index of polymers revealed by DOSY NMR. *Journal of Magnetic Resonance* **2011**, *212* (1), 169-173. DOI: https://doi.org/10.1016/j.jmr.2011.06.020.
(47) Dudás, E. F.; Bodor, A. Quantitative, Diffusion NMR Based Analytical Tool To Distinguish Folded, Disordered, and Denatured Biomolecules. *Anal Chem* **2019**, *91* (8), 4929-4933. DOI: 10.1021/acs.analchem.8b05617 From NLM.
(48) Tsarevsky, N. V.; Sumerlin, B. S.; Matyjaszewski, K. Step-Growth "Click" Coupling of Telechelic Polymers Prepared by Atom Transfer Radical Polymerization. *Macromolecules* **2005**, *38* (9), 3558-3561. DOI: 10.1021/ma050370d.
(49) Grieshaber, S. E.; Farran, A. J.; Lin-Gibson, S.; Kiick, K. L.; Jia, X. Synthesis and Characterization of Elastin-Mimetic Hybrid Polymers with Multiblock, Alternating Molecular Architecture and Elastomeric Properties. *Macromolecules* **2009**, *42* (7), 2532-2541. DOI: 10.1021/ma802791z From NLM.
(50) Grieshaber, S. E.; Farran, A. J.; Bai, S.; Kiick, K. L.; Jia, X. Tuning the properties of elastin mimetic hybrid copolymers via a modular polymerization method. *Biomacromolecules* **2012**, *13* (6), 1774-1786. DOI: 10.1021/bm3002705 From NLM.
(51) Wallimann, P.; Kennedy, R. J.; Miller, J. S.; Shalongo, W.; Kemp, D. S. Dual Wavelength Parametric Test of Two-State Models for Circular Dichroism Spectra of Helical Polypeptides: Anomalous Dichroic Properties of Alanine-Rich Peptides. *Journal of the American Chemical Society* **2003**, *125* (5), 1203-1220. DOI: 10.1021/ja0275360.
(52) Gazi, A. D.; Bastaki, M.; Charova, S. N.; Gkougkoulia, E. A.; Kapellios, E. A.; Panopoulos, N. J.; Kokkinidis, M. Evidence for a Coiled-coil Interaction Mode of Disordered Proteins from Bacterial Type III Secretion Systems*. *Journal of Biological Chemistry* **2008**, *283* (49), 34062-34068. DOI: https://doi.org/10.1074/jbc.M803408200.

(53) Ren, L.; Lu, X.; Li, W.; Yan, J.; Whittaker, A. K.; Zhang, A. Thermoresponsive Helical Dendronized Poly(phenylacetylene)s: Remarkable Stabilization of Their Helicity via Photo-Dimerization of the Dendritic Pendants. *Journal of the American Chemical Society* **2023**, *145* (45), 24906-24921. DOI: 10.1021/jacs.3c09333.
(54) Haider, M. J.; Zhang, H. V.; Sinha, N.; Fagan, J. A.; Kiick, K. L.; Saven, J. G.; Pochan, D. J. Self-assembly and soluble aggregate behavior of computationally designed coiled-coil peptide bundles. *Soft Matter* **2018**, *14* (26), 5488-5496, 10.1039/C8SM00435H. DOI: 10.1039/C8SM00435H.
(55) Sinha, N. J.; Wu, D.; Kloxin, C. J.; Saven, J. G.; Jensen, G. V.; Pochan, D. J. Polyelectrolyte character of rigid rod peptide bundlemer chains constructed via hierarchical self-assembly. *Soft Matter* **2019**, *15* (48), 9858-9870, 10.1039/C9SM01894H. DOI: 10.1039/C9SM01894H.
(56) Sinha, N. J.; Shi, Y.; Tang, Y.; Kloxin, C. J.; Saven, J. G.; Faraone, A.; Jensen, G. V.; Pochan, D. J. Intramolecular structure and dynamics in computationally designed peptide-based polymers displaying tunable chain stiffness. *Physical Review Materials* **2021**, *5* (9), 095601. DOI: 10.1103/PhysRevMaterials.5.095601.
(57) des Cloizeaux, J. J., G. *Polymers in Solution: Their Modelling and Structure*; Oxford Science Publications, 1991.
(58) Sautaux, J.; Marx, F.; Gunkel, I.; Weder, C.; Schrettl, S. Mechanically robust supramolecular polymer co-assemblies. *Nature Communications* **2022**, *13* (1), 356. DOI: 10.1038/s41467-022-28017-0.
(59) Peng, Y. H.; Hsiao, S. K.; Gupta, K.; Ruland, A.; Auernhammer, G. K.; Maitz, M. F.; Boye, S.; Lattner, J.; Gerri, C.; Honigmann, A.; et al. Dynamic matrices with DNA-encoded viscoelasticity for cell and organoid culture. *Nature Nanotechnology* **2023**, *18*, 1463-1473. DOI: 10.1038/s41565-023-01483-3.
(60) Lang, P.; Frey, E. Disentangling entanglements in biopolymer solutions. *Nat Commun* **2018**, *9* (1), 494. DOI: 10.1038/s41467-018-02837-5 From NLM.